Science Advances
AAAS

Supplementary Materials for

Biphasic regulation of epigenetic state by matrix stiffness during cell reprogramming

Yang Song *et al.*

Corresponding author: Song Li, songli@ucla.edu

Sci. Adv. **10**, eadk0639 (2024)
DOI: 10.1126/sciadv.adk0639

This PDF file includes:

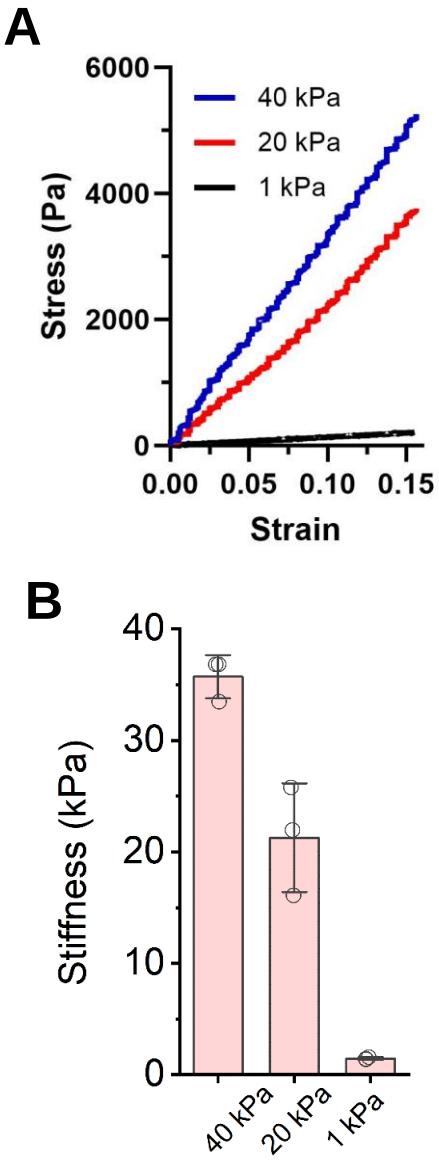

Fig. S1. Mechanical characterization of polyacrylamide (PAAm) gels. PAAm gels of varying stiffness were fabricated, and subjected to compression testing to determine the mechanical properties. **(A)** Stress-strain curves showing the linear elastic property of the gels. **(B)** The elastic modulus/stiffness of the gels was calculated based on the experimental data exemplified in **A** (n=3) . Bar graph shows mean ± standard deviation (SD).

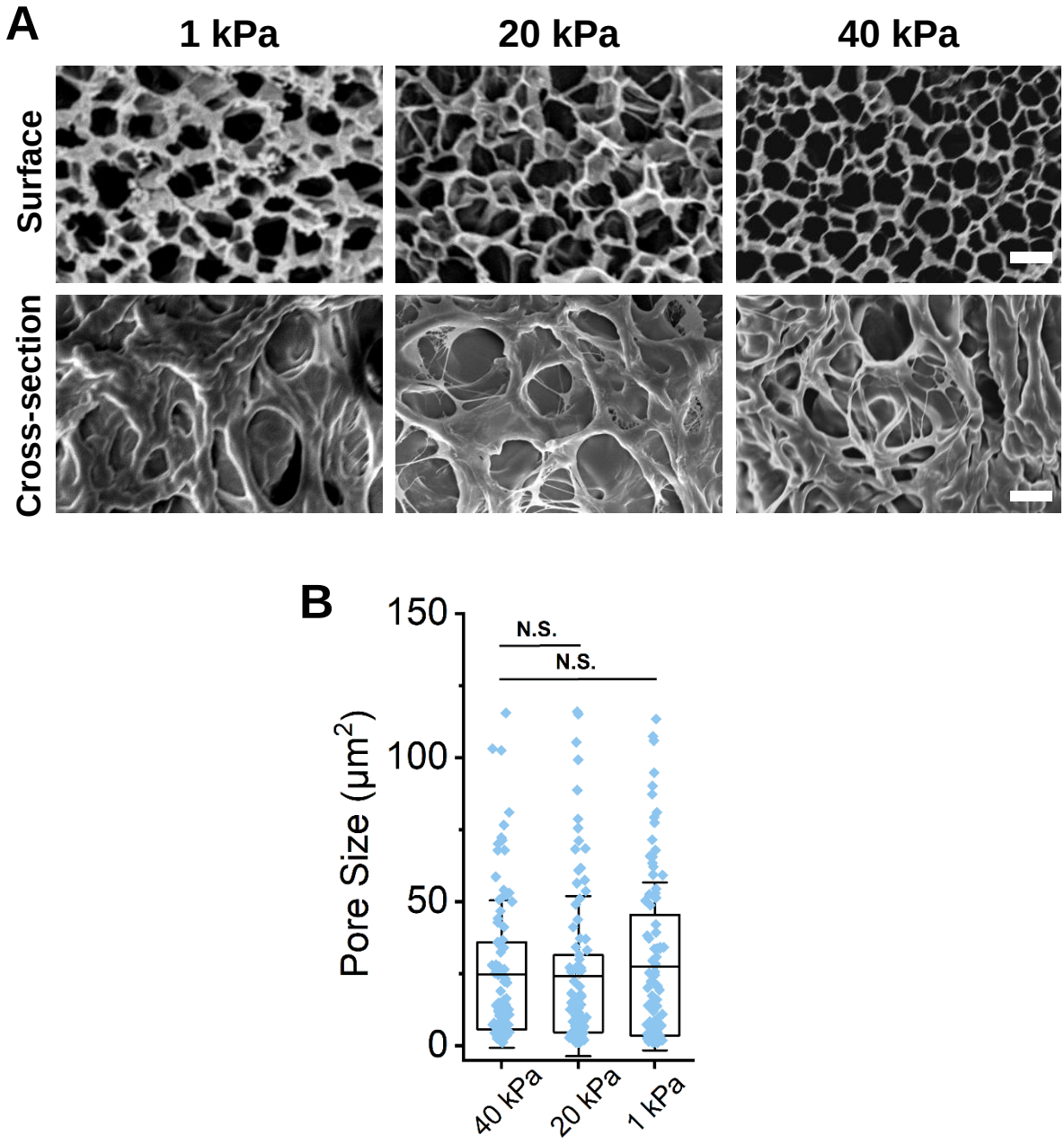

Fig. S2. Surface and cross-sectional properties of PAAm gels. (A) Scanning electron microscopy images of the surface and cross-sections of PAAm gels with different stiffness. Scale bar, 10 μm. **(B)** Quantification of pore size based on SEM images in **A** (n=100). Statistical significance was determined by a one-way ANOVA and Tukey's multiple comparison test (N.S.: not significant). Box plots show the ends at the quartiles, the mean as a horizontal line in the box, and the whiskers represent the standard deviation (SD).

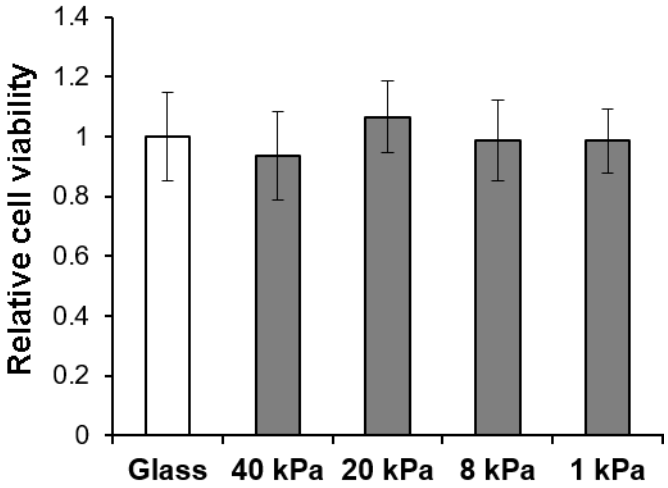

Fig. S3. Effect of PAAm gels on cell viability. Quantification of cell viability of fibroblasts cultured (relative to cells on glass) on PAAm gels of various stiffness after 24 hours, as determined by the PrestoBlue assay (n=3). Statistical significance was determined by a one-way ANOVA and Tukey's multiple comparison test. No statistical difference was observed among groups. Bar graph shows mean ± SD.

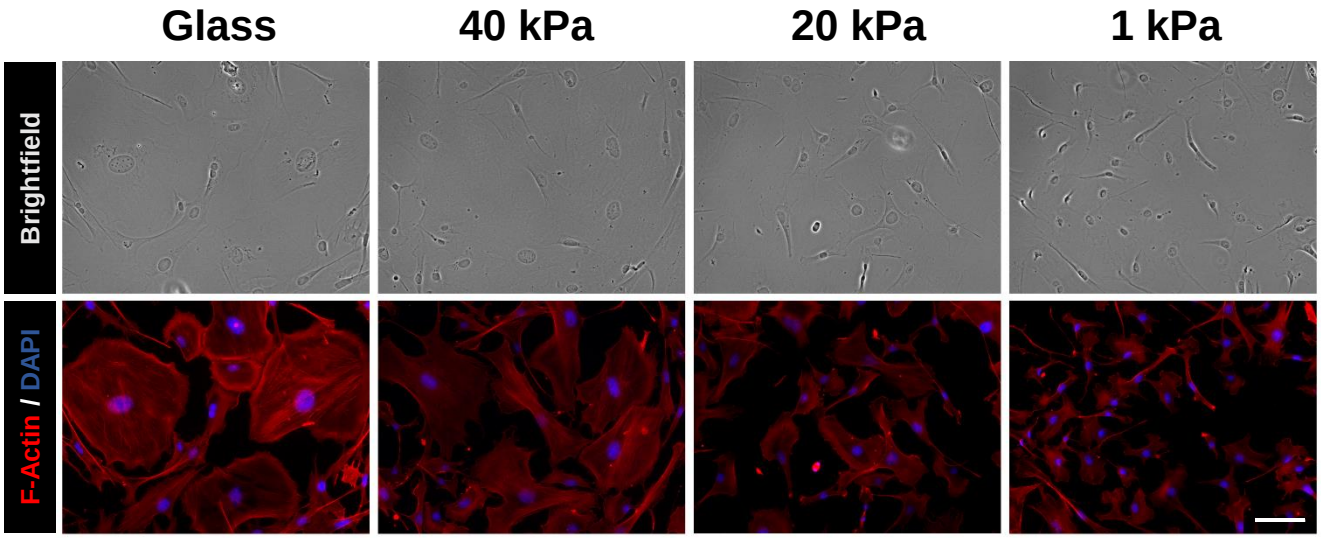

Fig. S4. Effect of matrix stiffness on cell spreading. Brightfield (top) or immunofluorescent (bottom) images of fibroblasts cultured on glass or PAAm gels of varying stiffness for 2 days. Immunofluorescent images show the actin network (phalloidin, red) and nuclei (DAPI, blue) of fibroblasts in response to matrix stiffness. Scale bar, 100 μm.

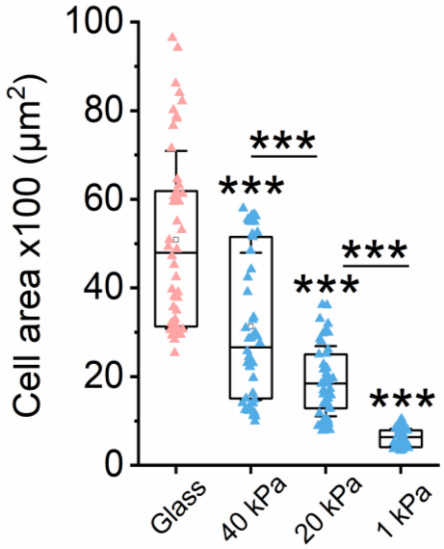

Fig. S5. Effect of matrix stiffness on cell area. Quantification of cell area based on phalloidin staining (n>50 cells from at least 3 independently prepared gel surfaces). Fibroblasts were seeded onto polyacrylamide (PAAm) gels of varying stiffness or glass, which served as control in all experiments, for 24 hours. Statistical significance was determined by a one-way ANOVA and Tukey's multiple comparison test (***p<0.001). Box plots show the ends at the quartiles, the mean as a horizontal line in the box, and the whiskers represent the standard deviation (SD).

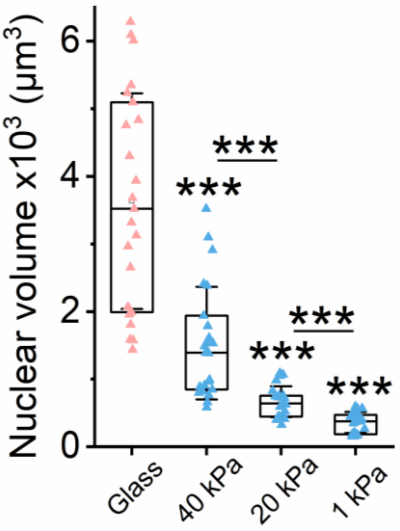

Fig. S6. Effect of matrix stiffness on nuclear volume. Quantification of nuclear volume based on DAPI staining and confocal microscopy from fibroblasts cultured of PAAm gels or glass for 24 hours (n>30 cells from 3 independently prepared gel surfaces). Statistical significance was determined by a one-way ANOVA and Tukey's multiple comparison test (***p<0.001). Box plots show the ends at the quartiles, the mean as a horizontal line in the box, and the whiskers represent the standard deviation (SD).

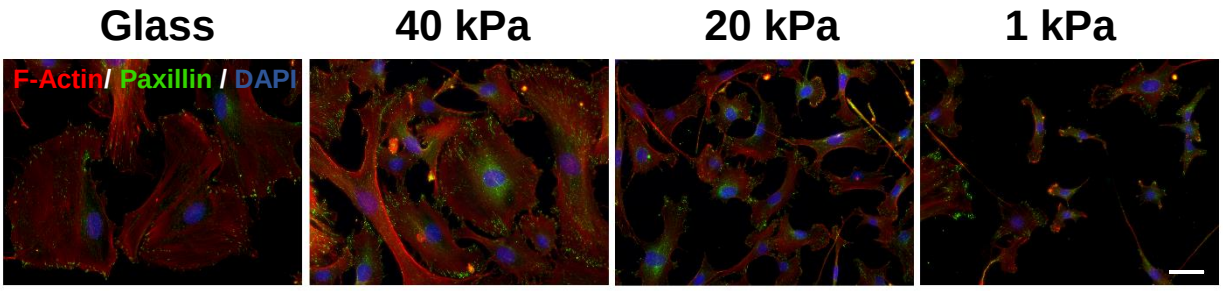

Fig. S7. Effect of matrix stiffness on focal adhesions. Immunofluorescent images of paxillin expression in fibroblasts cultured on glass or matrices of varying stiffness for 2 days. Scale bar, 50 μm.

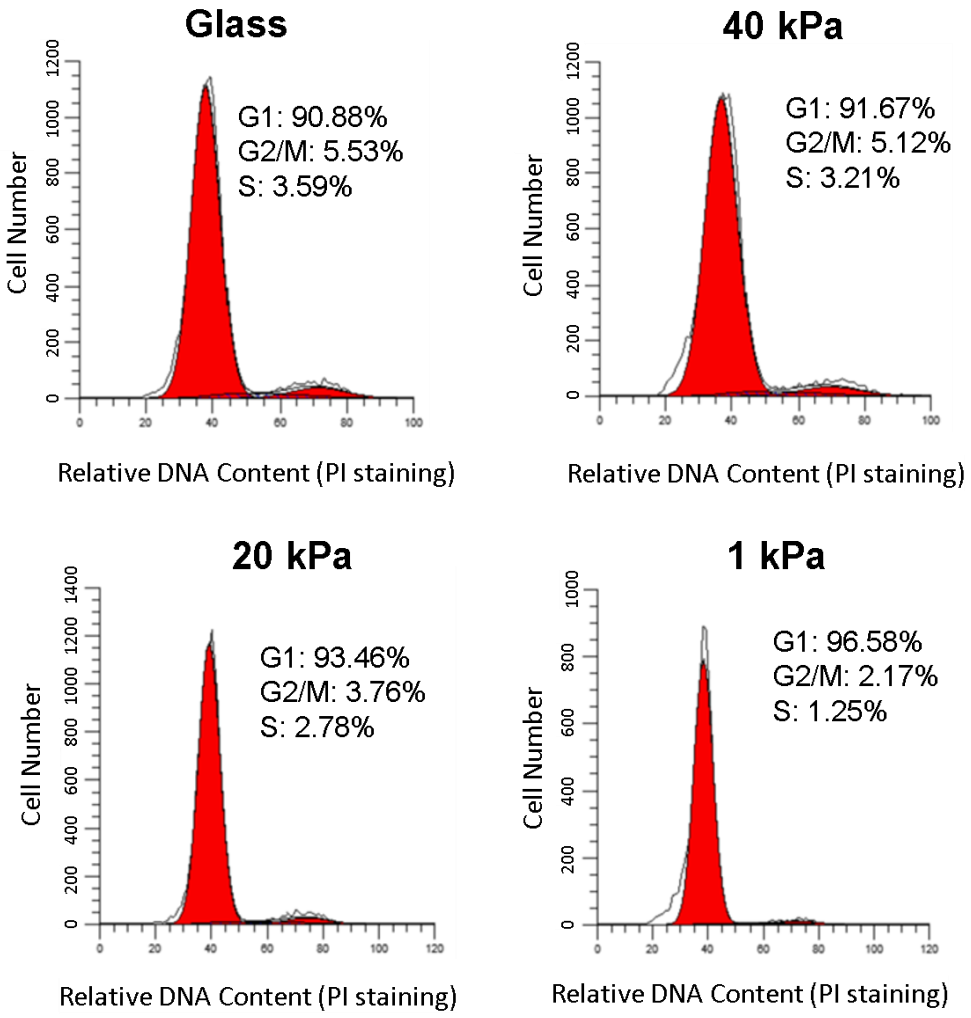

Fig. S8. Effect of matrix stiffness on the cell cycle of fibroblasts. Mouse fibroblasts were seeded on fibronectin-coated glass and PAAm gels with varying stiffness for 48 hours. Cells were collected and stained with propidium iodide, and DNA contents were analyzed by flow cytometry.

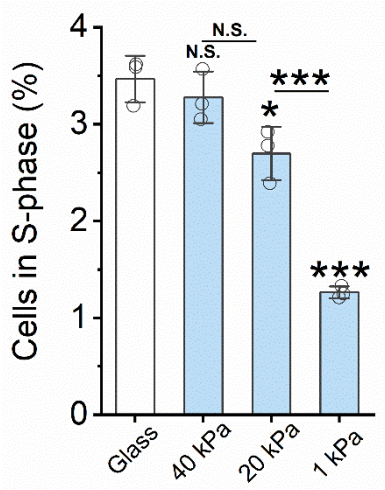

Fig. S9. Effect of matrix stiffness on the cell cycle of fibroblasts. The percentage of cells in the S-phase of the cell cycle based on propidium iodide staining. Fibroblasts were seeded on PAAm gels for 48 hours, collected and stained with propidium iodide followed by flow cytometry analysis (n=3 independently prepared gel surfaces). Statistical significance was determined by a one-way ANOVA and Tukey's multiple comparison test (N.S.: not significant, ***$p<0.001$). Bar graph shows mean ± SD.

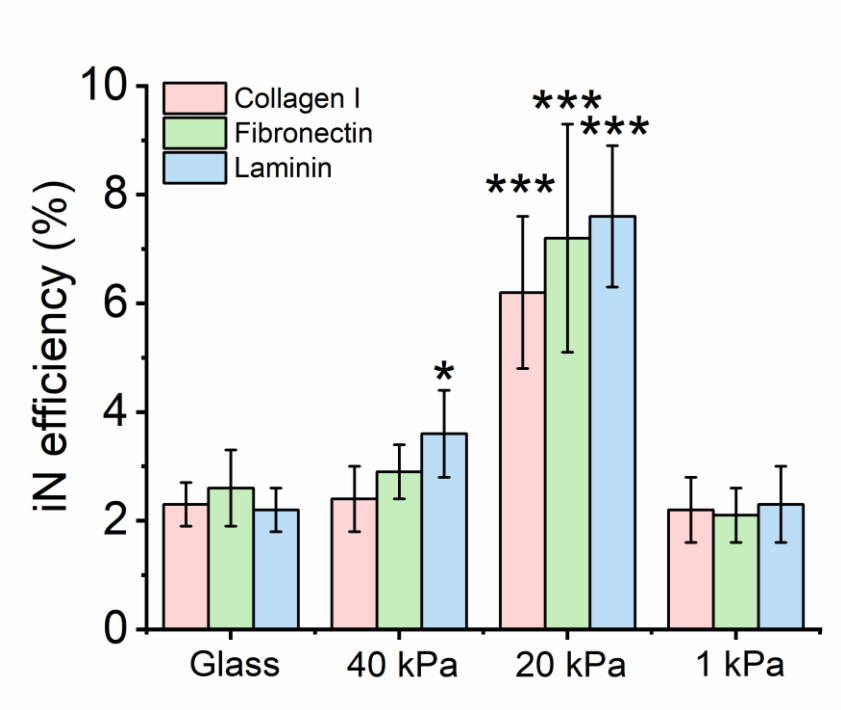

Fig. S10. Effect of extracellular matrix (ECM) coating on substrate stiffness-mediated iN reprogramming. Reprogramming efficiency of BAM-transduced fibroblasts cultured on PAAm gels of varying stiffness and coated with different extracellular matrix proteins (n=3 independently prepared gel surfaces). At day 7, the cells were fixed and stained for Tubb3 by Tuj1 antibody, followed by immunofluorescence microscopy to quantify $Tubb3^{+}$ iN cells. Cells cultured on glass were kept as a control. Statistical significance was determined by a one-way ANOVA and Tukey's multiple comparison test (*$p<0.05$, ***$p<0.001$). Bar graph shows mean ± SD.

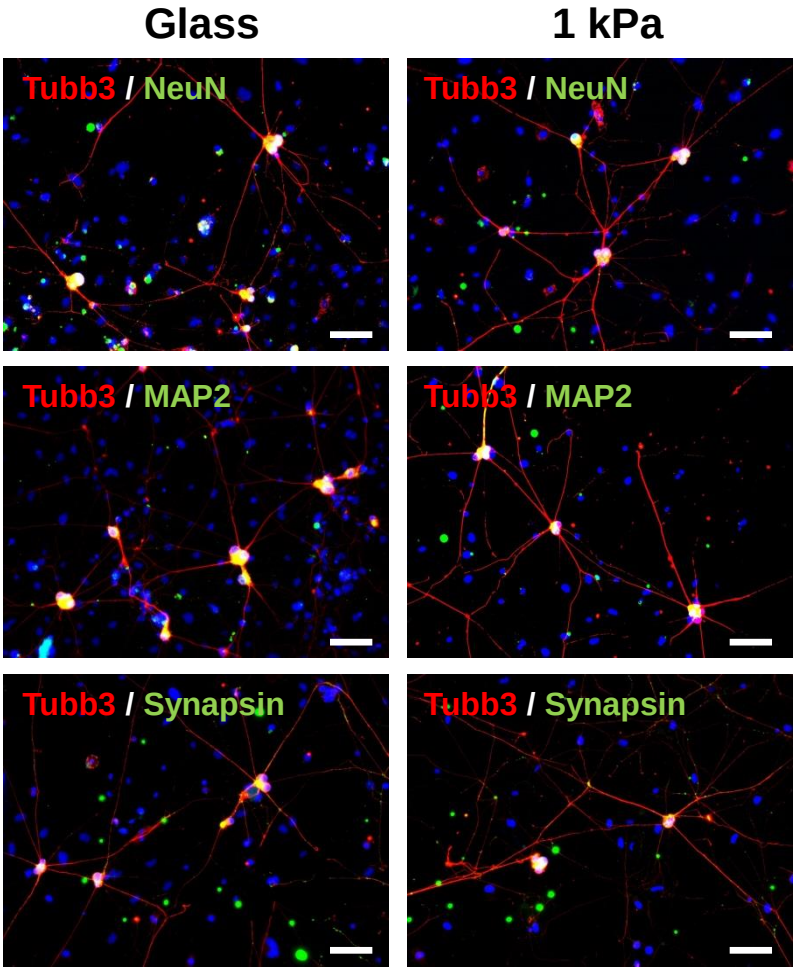

Fig. S11. Substrate stiffness-induced iN cells express mature markers. Immunofluorescent mages of $Tubb3^{+}$ iN cells on glass and 1 kPa gels expressing mature neuronal markers, microtubule associated protein 2 (MAP2) and synapsin after 21 days. Scale bar, 100 μm.

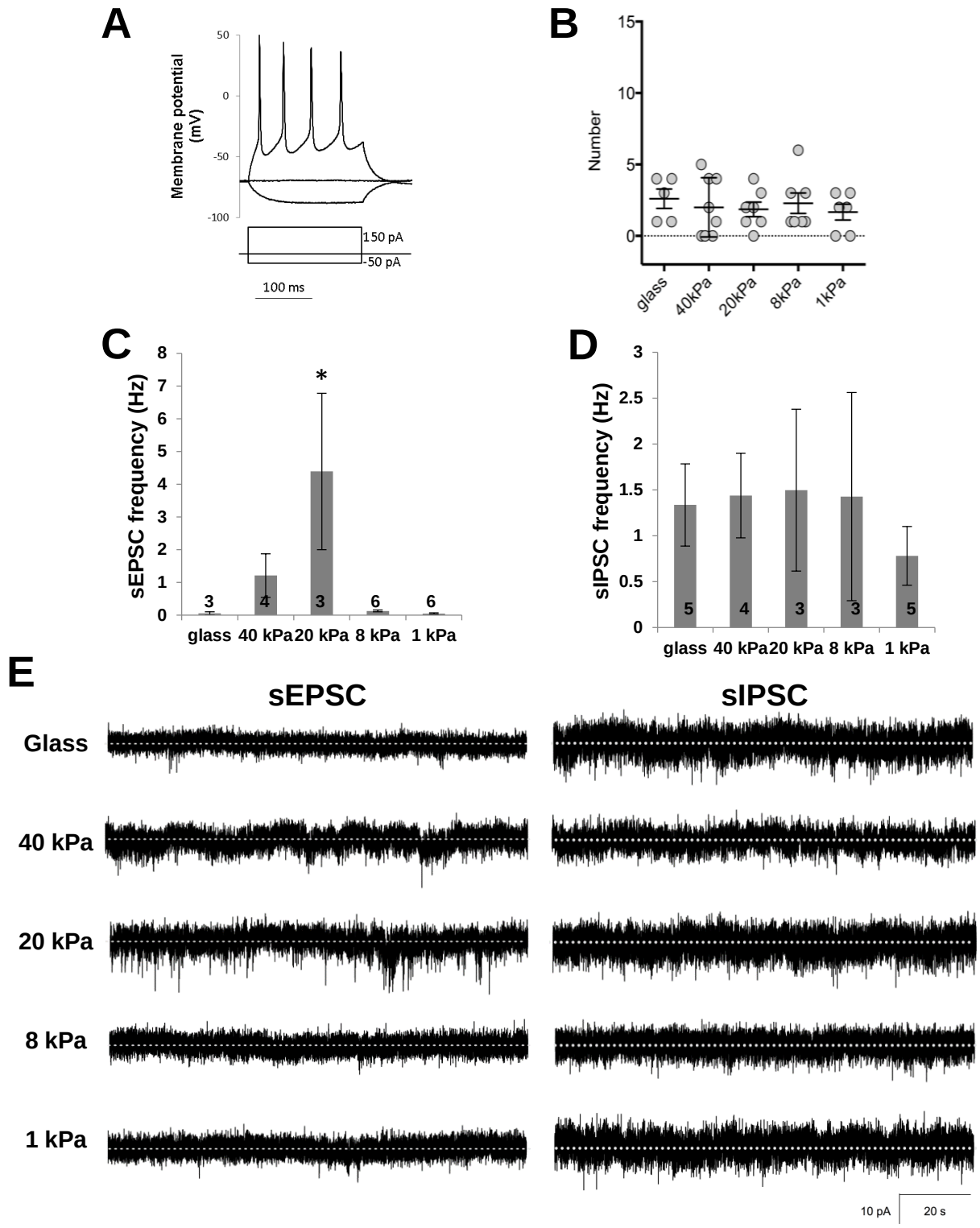

Fig. S12. Electrophysiology analysis indicating iN cell functionality. (A) Representative trace showing spontaneous changes in membrane potential in response to current injection from iN cells on glass. **(B)** Number of action potentials generated per iN cells across all stiffness. Each circle represents one cell tested. **(C)** Quantification of spontaneous excitatory postsynaptic current (sEPSC) frequency of iNs across all stiffness (*$p \leq 0.05$). Number of iNs tested as stated. **(D)** Quantification of spontaneous inhibitory postsynaptic current (sIPSC) frequency of iNs across all stiffness. Number of iNs tested as stated. **(E)** Representative sEPSC and sIPSC traces generated from iNs across all surfaces. Bar graphs represent mean ± one standard error of mean. Statistical significance determined by one-way ANOVA followed by Dunnett's post-hoc test, compared to glass.

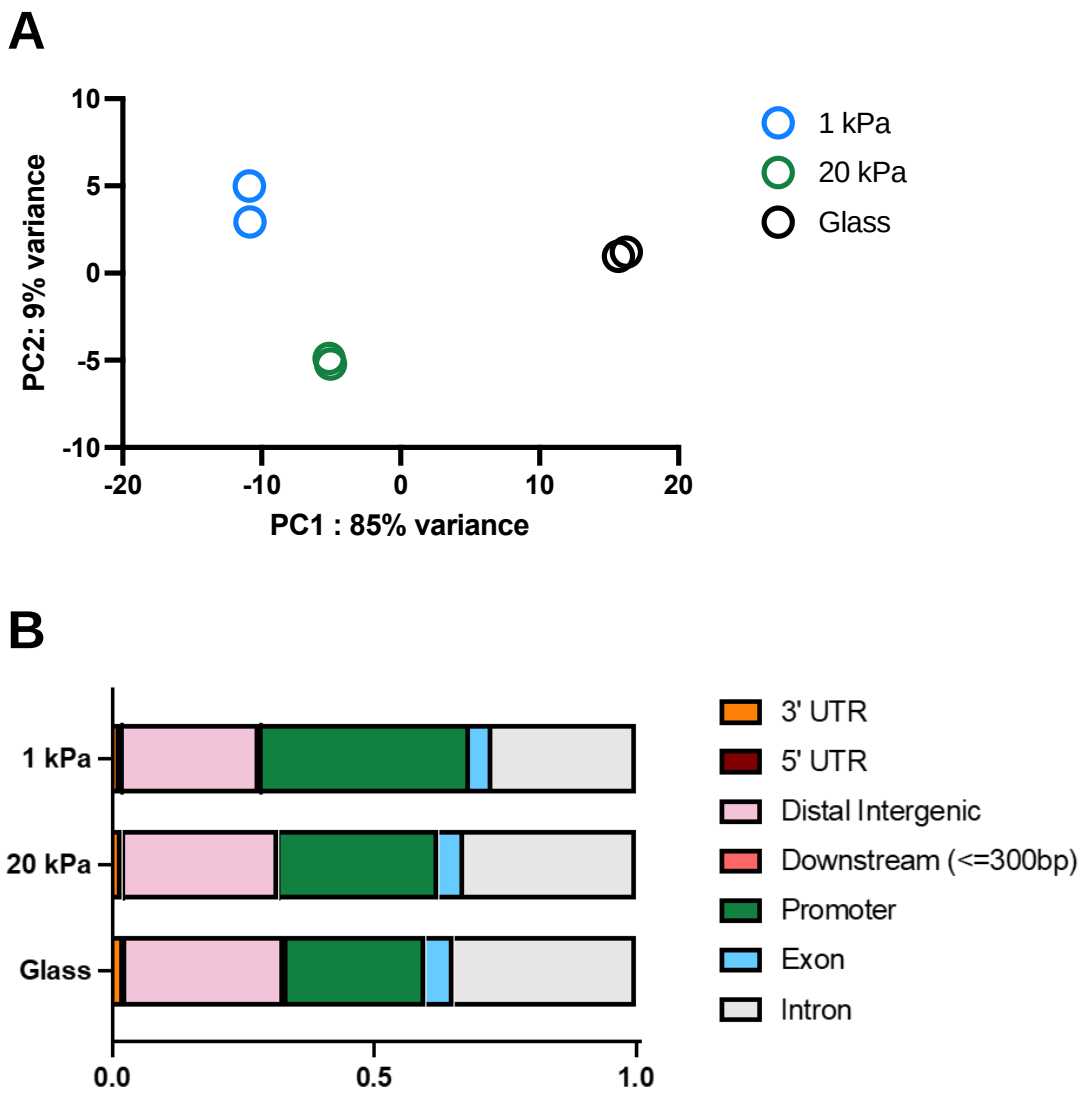

Fig. S13. Effect of substrate stiffness on chromatin accessibility. (a) Principal component analysis (PCA) of ATAC-seq data from independent biological replicates of fibroblasts cultured on PAAm gels for 3 days (n=2). **(b)** Genomic annotations of ATAC peaks for the indicated conditions.

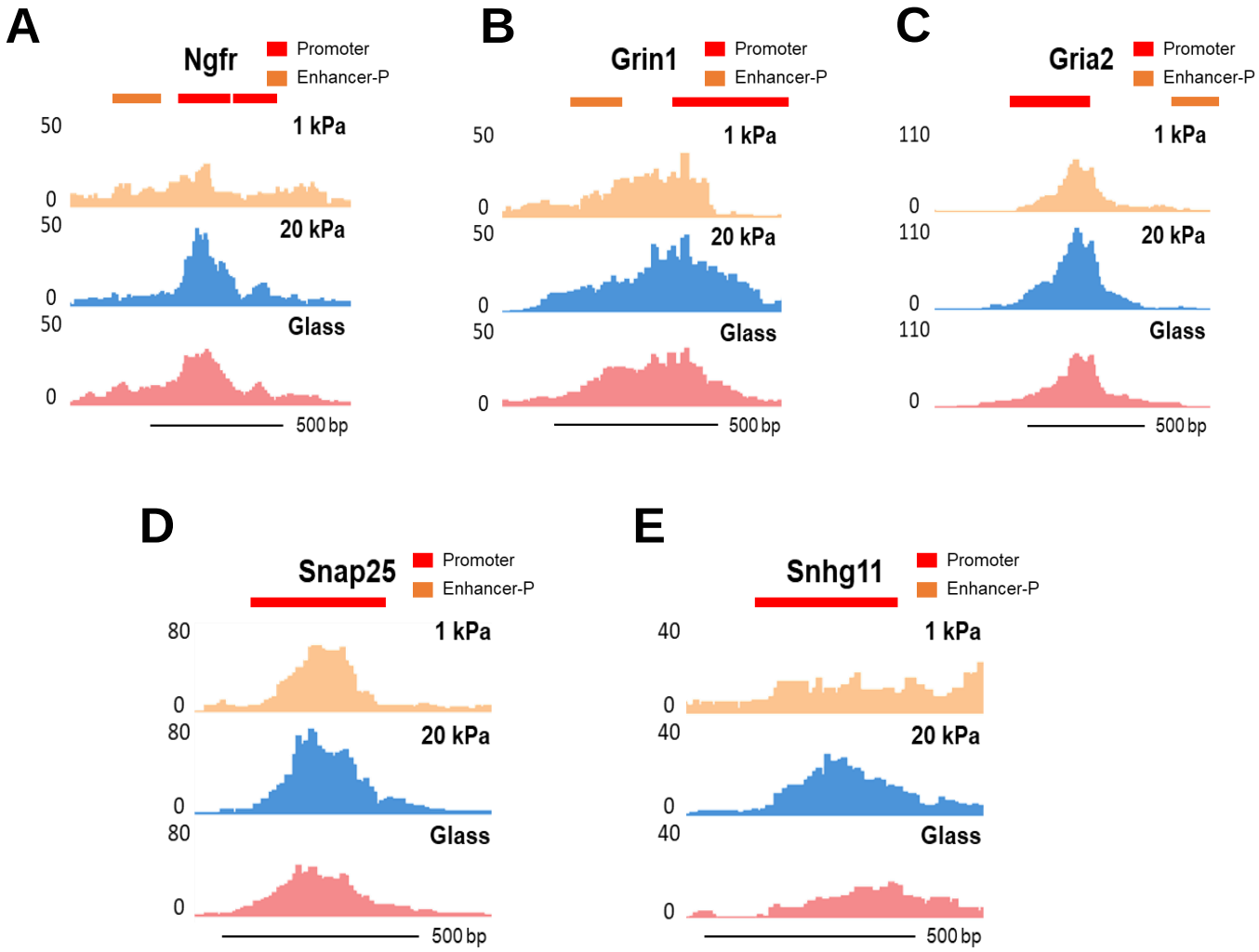

Fig. S14. Matrix stiffness altered chromatin accessibility around Ascl1-target genomic loci. (A-E) Representative ATAC-seq tracks for *Ngfr, Grin1*, *Gria2*, *Snap25*, and *Snhg11* genomic loci from fibroblasts cultured on varying matrix stiffness for 3 days. Intermediate stiffness promotes chromatin accessibility near promoter and proximal enhancer (Enhancer-P) sites of *Ascl1*-target genes.

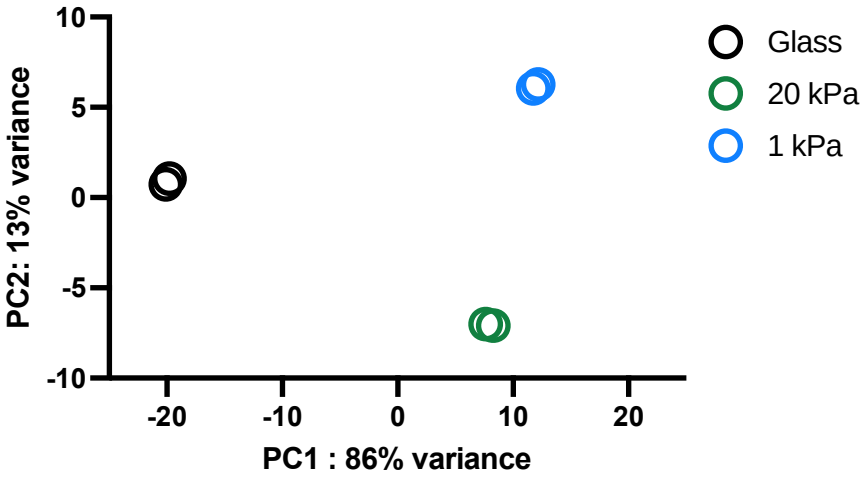

Fig. S15. Effect of substrate stiffness on gene expression. Principal component analysis (PCA) of bulk RNA-seq data from independent biological replicates of fibroblasts cultured on PAAm gels for 3 days (n=2).

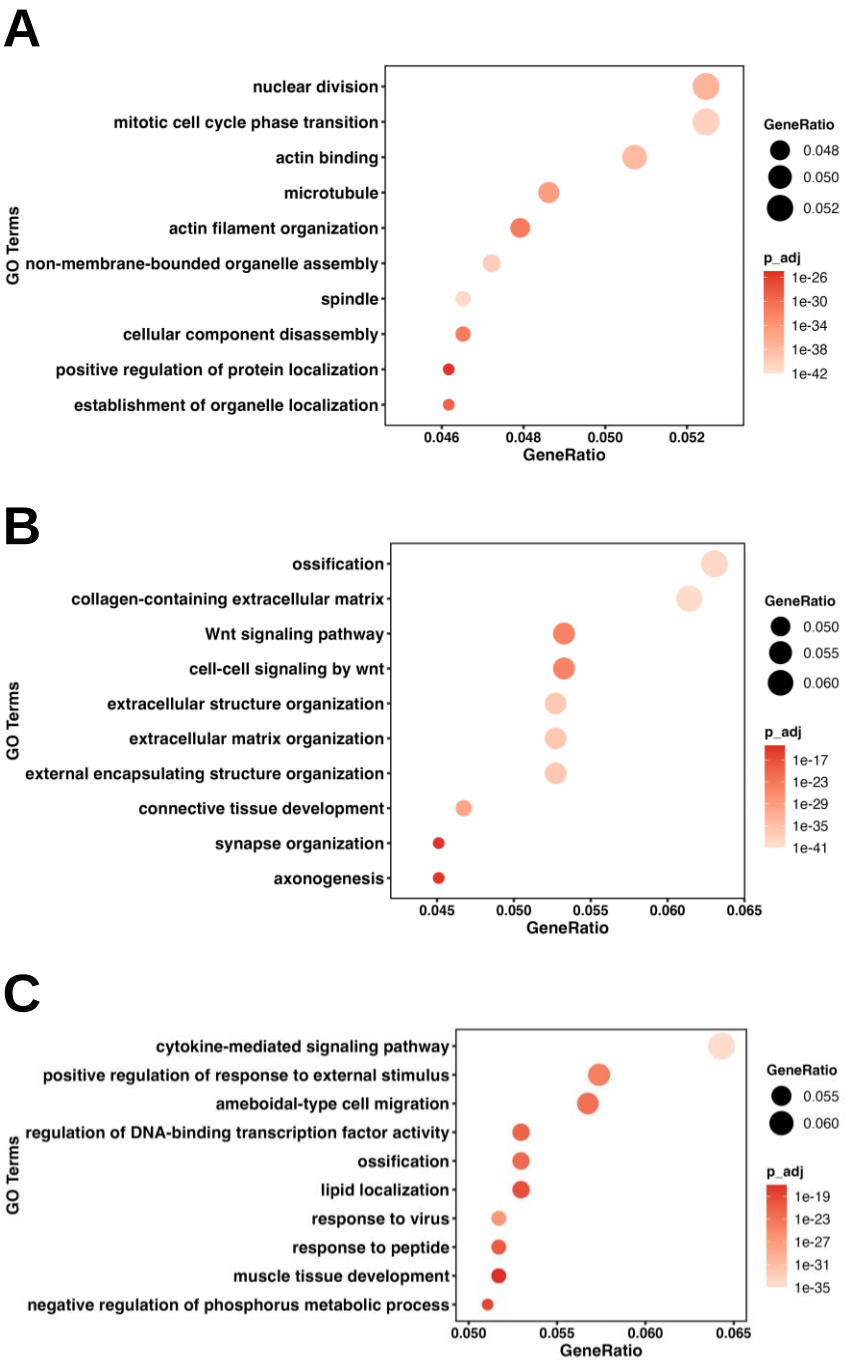

Fig. S16. Effect of substrate stiffness on gene expression. (A-C) Top 10 gene ontology (GO) terms for highly expressed genes in samples of fibroblasts cultured on glass (**A**), 20 kPa gels (**B**), and 1 kPa gels (**C**) for 3 days based on RNA sequencing (n=2).

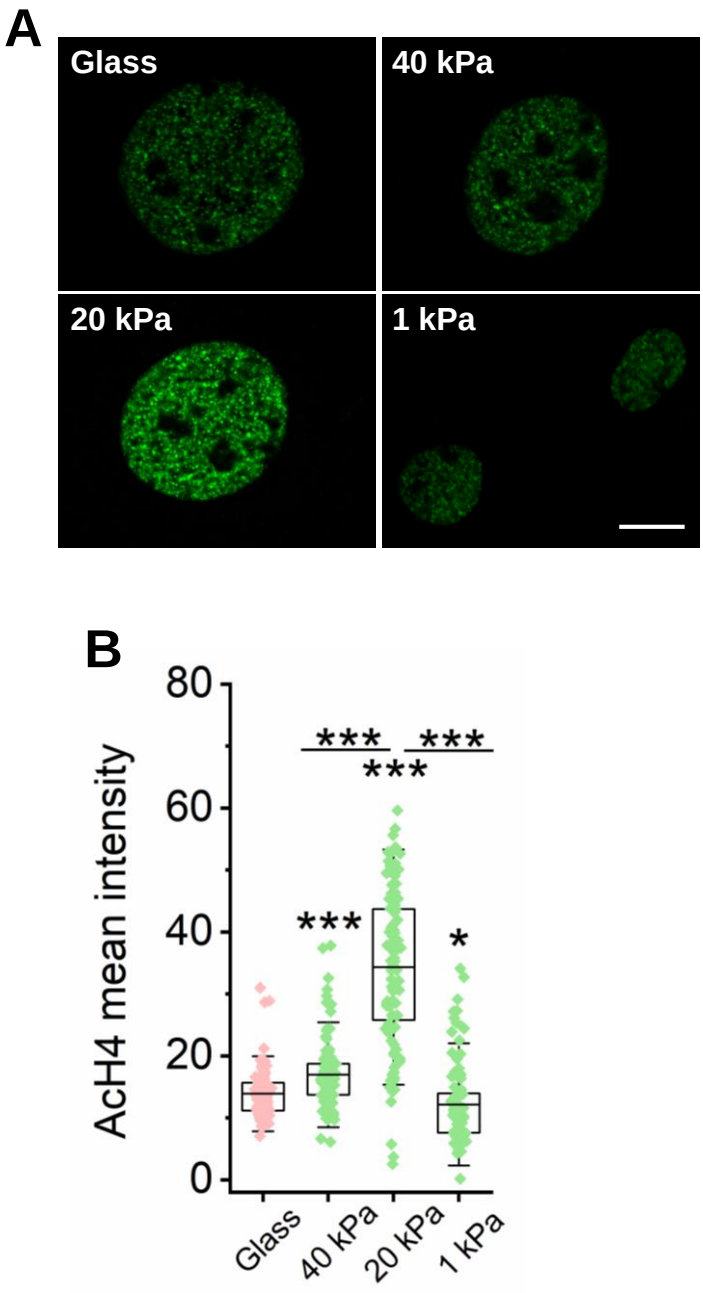

Fig. S17. Effect of substrate stiffness on global levels of histone H4 acetylation (AcH4). (A) Representative immunofluorescent images show the level and distribution of AcH4 marks in non-transduced fibroblasts cultured on glass and PAAm gels of varying stiffness for 2 days. Scale bar, 5 µm. **(B)** Quantification of AcH4 intensity in cells cultured on glass and PAAm gels of various stiffness (based on experiments in **a**) (n=100 cells from at least 3 independently prepared gel surfaces). Statistical significance was determined by a one-way ANOVA and Tukey's multiple comparison test (*$p<0.05$, ***$p<0.001$). Box plots show the ends at the quartiles, the mean as a horizontal line in the box, and the whiskers represent the standard deviation (SD).

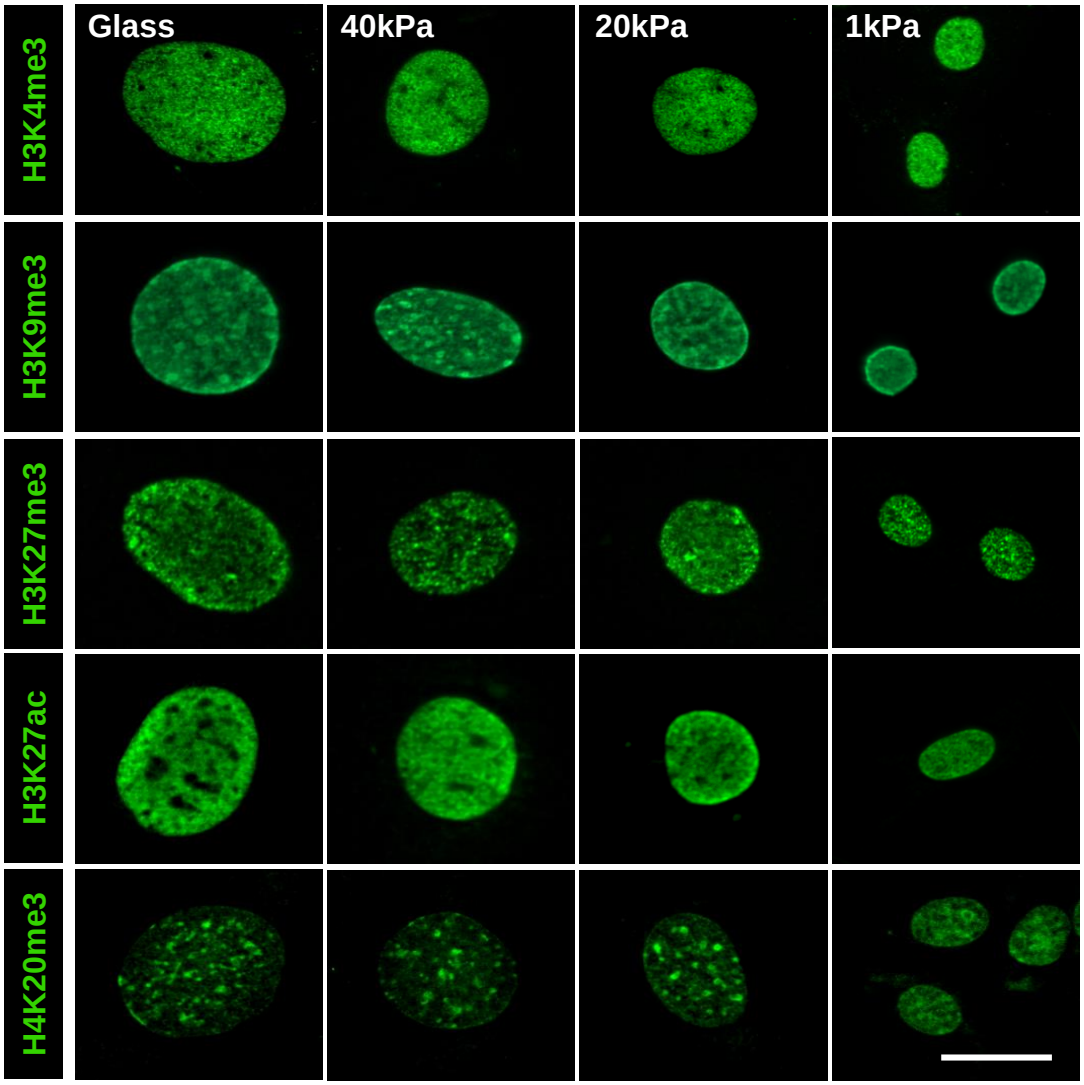

Fig. S18. Effect of substrate stiffness on global levels of histone marks. Representative immunofluorescent images show the level and distribution of various histone marks in non-transduced fibroblasts cultured on glass and PAAm gels of varying stiffness for 2 days. Scale bar, 10 μm.

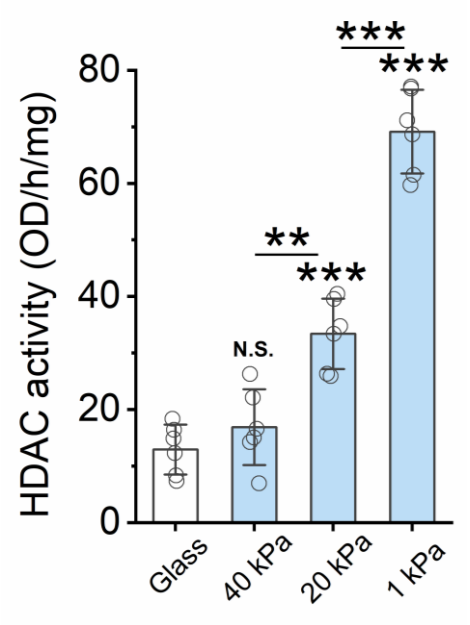

Fig. S19. Effect of substrate stiffness on histone deacetylase (HDAC) activity. Quantification of HDAC activity in fibroblasts seeded on glass and PAAm gels of various stiffness for 2 days, as determined using the Epigenase HDAC activity assay kit (n=6). Cells cultured on glass were kept as a control. Statistical significance was determined by a one-way ANOVA and Tukey's multiple comparison test (N.S.: not significant, **p<0.01, ***p<0.001). Bar graph shows mean ± SD.

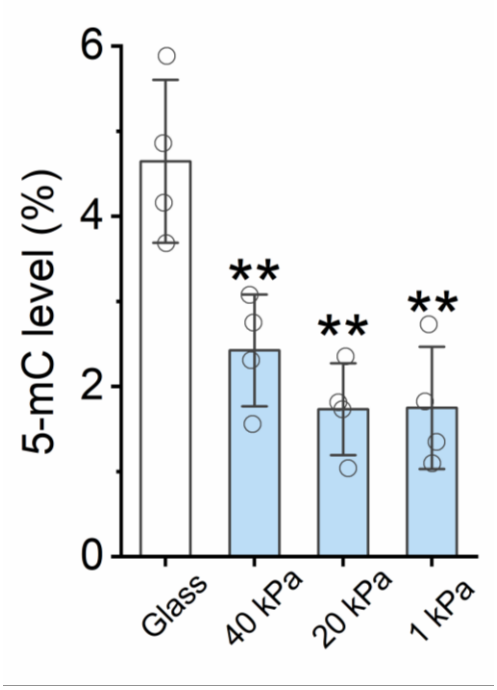

Fig. S20. Effect of substrate stiffness on DNA methylation. Quantification of 5-mC level in fibroblasts seeded on glass and PAAm gels of various stiffness for 2 days, as determined using the MethylFlash™ Global DNA Methylation (5-mC) ELISA Easy Kit (n=4). Cells cultured on glass were kept as a control. Statistical significance was determined by a one-way ANOVA and Tukey's multiple comparison test (**$p<0.01$). Bar graph shows mean ± SD.

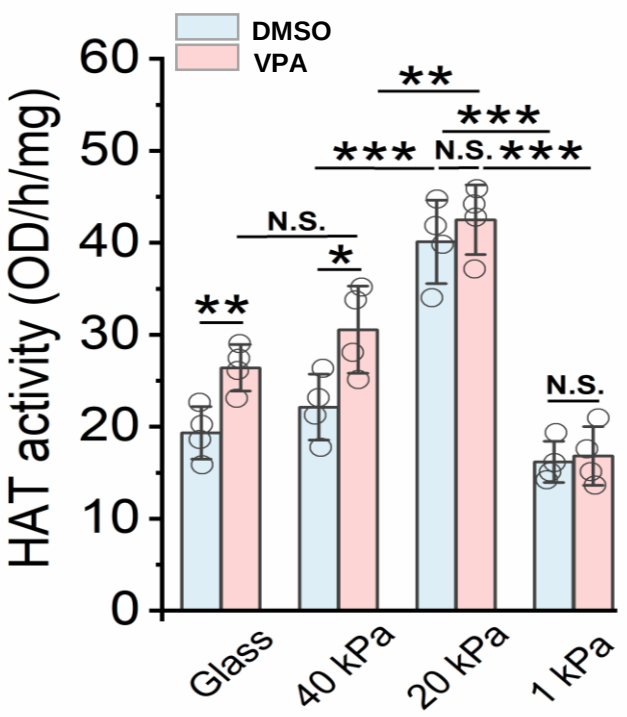

Fig. S21. Effect of histone deacetylase (HDAC) inhibition on histone acetyltransferase (HAT) activity. Quantification of HAT activity in fibroblasts seeded on glass and PAAm gels of various stiffness for 1 day, followed by treatment with vehicle control (DMSO) or an HDAC inhibitor (valproic acid) for 24 hours, as determined using the Epigenase HAT activity assay kit (n=4). Cells cultured on glass were kept as a control. Statistical significance was determined by a one-way ANOVA and Tukey's multiple comparison test (N.S.: not significant, *p<0.05, **p<0.01, ***p<0.001). Bar graph shows mean ± SD.

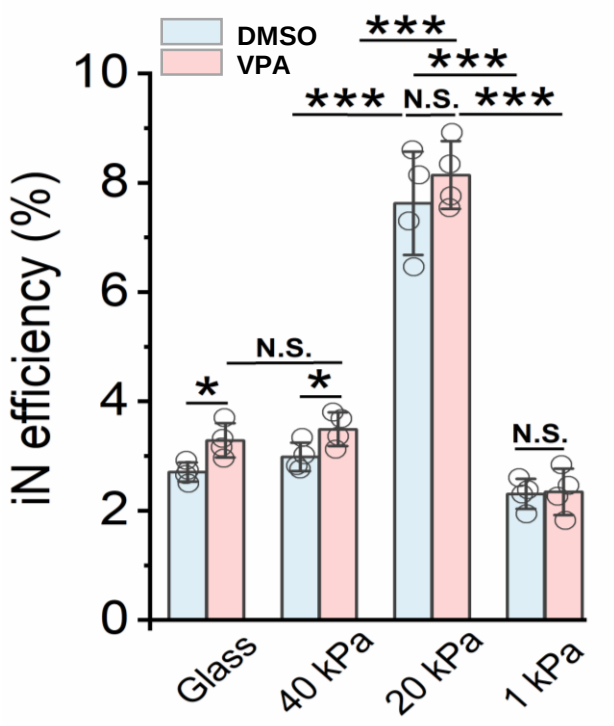

Fig. S22. Effect of histone deacetylase inhibition on iN reprogramming efficiency. Reprogramming efficiency of BAM-transduced fibroblasts cultured on matrices of varying stiffness and pre-treated with 500 μM HDAC inhibitor, valproic acid (VPA), for 24 hours before the addition of Dox (n=4). At day 7, the cells were fixed and stained for Tubb3 by Tuj1 antibody, followed by immunofluorescence microscopy to quantify $Tubb3^{+}$ iN cells. Cells cultured on glass were kept as a control. Statistical significance was determined by a one-way ANOVA and Tukey's multiple comparison test (NS: not significant, *$p<0.05$, ***$p<0.001$). Bar graph shows mean ± SD.

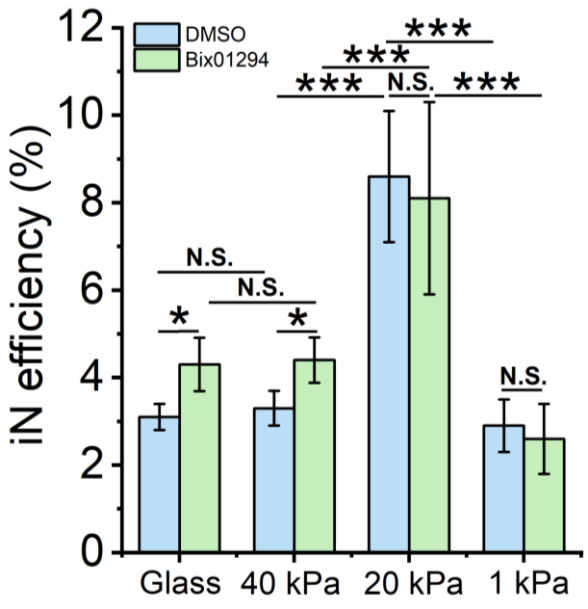

Fig. S23. Effect of histone methyltransferase (HMT) inhibition on iN reprogramming efficiency. Reprogramming efficiency of BAM-transduced fibroblasts cultured on matrices of varying stiffness and pre-treated with 1 μM HMT inhibitor, Bix01294, for 24 hours before the addition of Dox (n=3). At day 7, the cells were fixed and stained for Tubb3 by Tuj1 antibody, followed by immunofluorescence microscopy to quantify $Tubb3^{+}$ iN cells. Cells cultured on glass were kept as a control. Statistical significance was determined by a one-way ANOVA and Tukey's multiple comparison test (NS: not significant, *$p<0.05$, ***$p<0.001$). Bar graph shows mean ± SD.

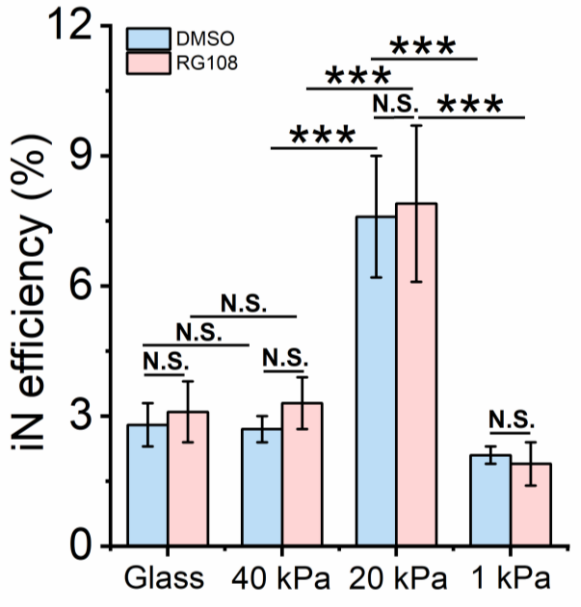

Fig. S24. Effect of DNA methyltransferase inhibition on iN reprogramming efficiency. Reprogramming efficiency of BAM-transduced fibroblasts cultured on matrices of varying stiffness and pre-treated with 20 μM DNMT inhibitor, RG108, for 24 hours before the addition of Dox (n=3). At day 7, the cells were fixed and stained for Tubb3 by Tuj1 antibody, followed by immunofluorescence microscopy to quantify Tubb3^{+} iN cells. Cells cultured on glass were kept as a control. Statistical significance was determined by a one-way ANOVA and Tukey's multiple comparison test (NS: not significant, ***$p<0.001$). Bar graph shows mean ± SD.

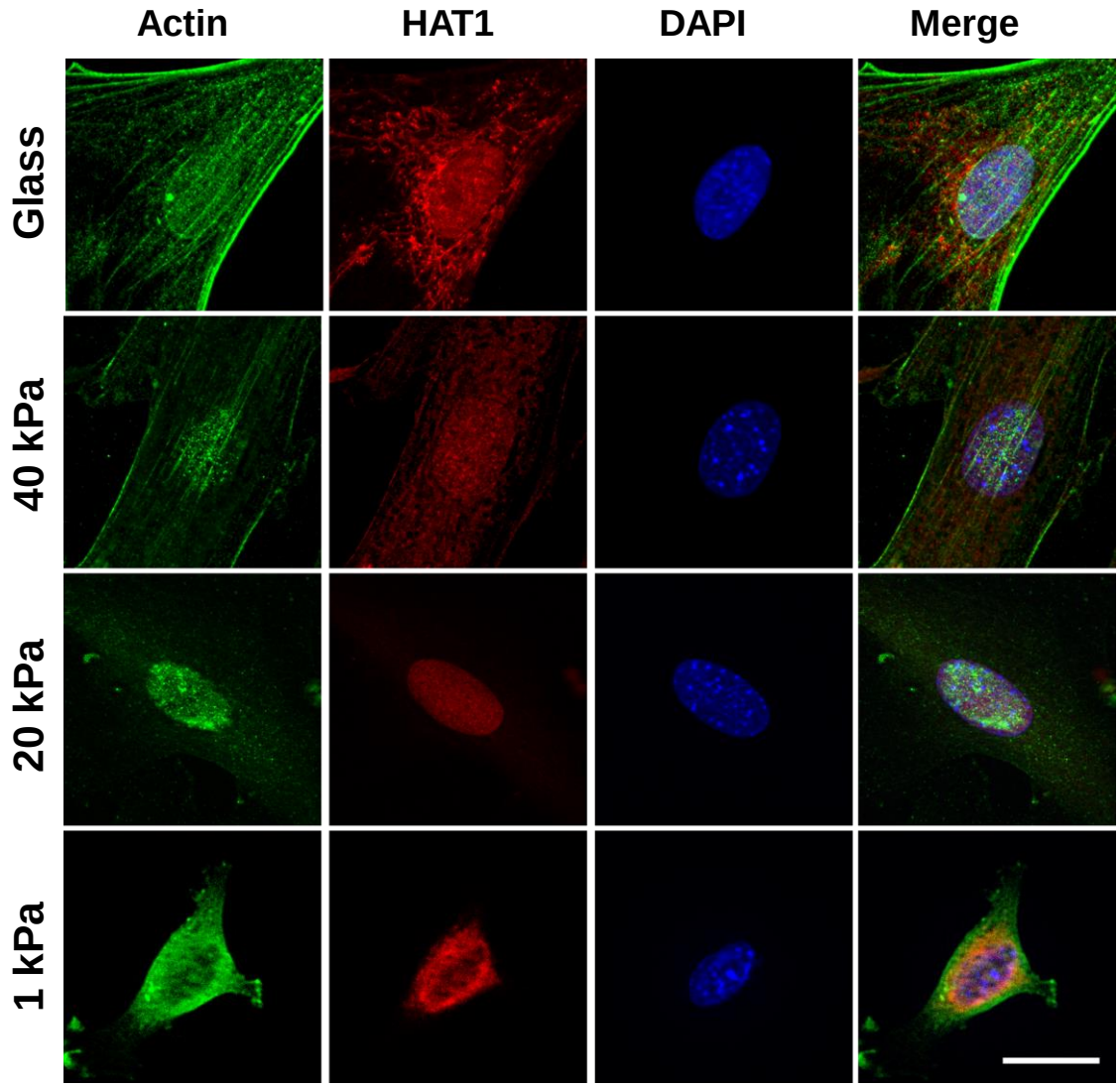

Fig. S25. Matrix stiffness modulates HAT1 localization by regulating actin assembly. Representative images of pan-actin (green) and HAT1 (red) in fibroblasts cultured on glass and PAAm gels of varying stiffness for 2 days. Scale bar, 10 μm.

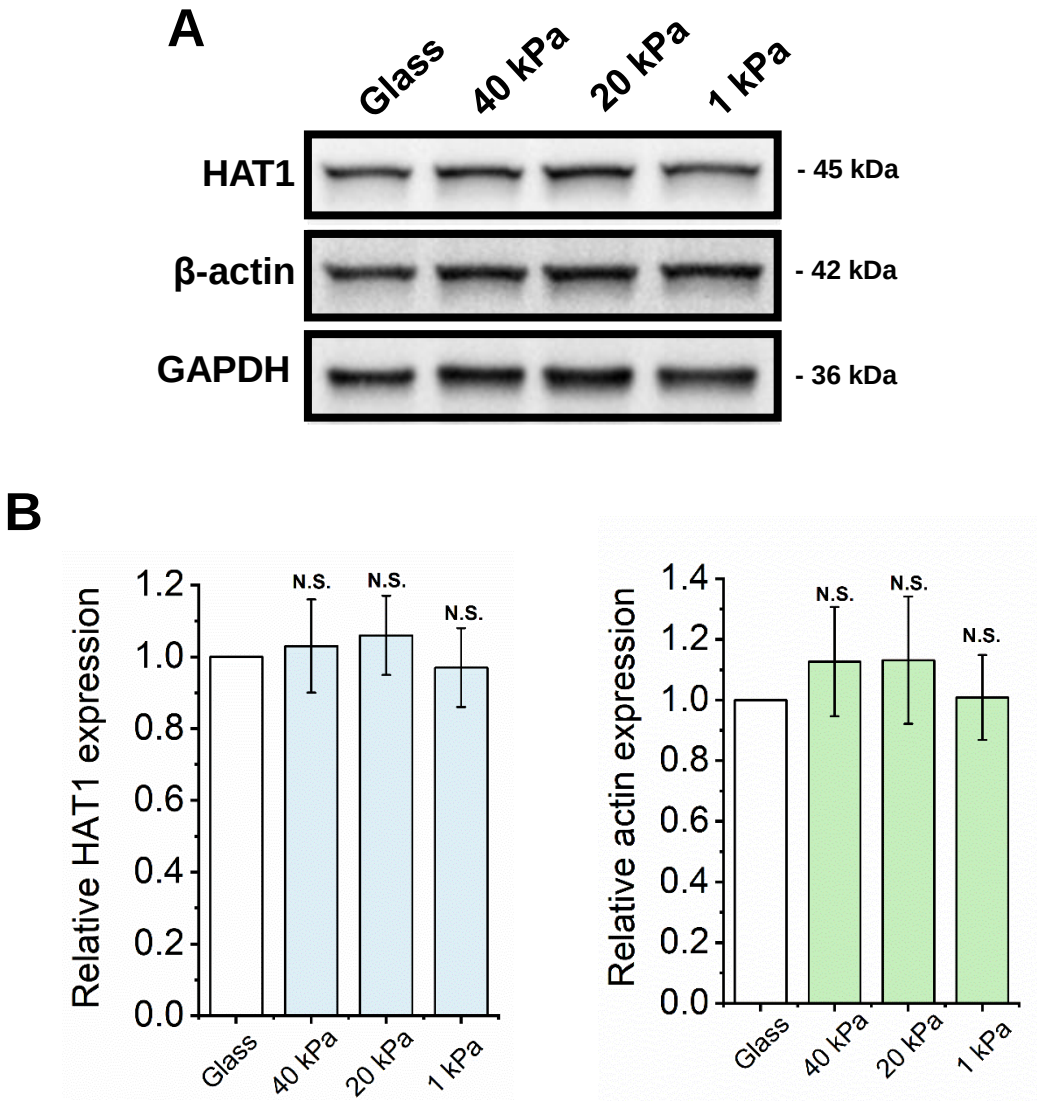

Fig. S26. Effect of matrix stiffness on HAT1 and actin levels. **(A)** Western blotting analysis shows HAT1 and pan-actin levels from whole cell lysates of fibroblasts cultured on glass and PAAm gels for 2 days, where GAPDH acts as housekeeping protein. **(B)** Quantification of HAT1 and pan-actin level from Western blots in **A** (n=3), where protein levels were normalized to GAPDH. Cells seeded on glass served as a control. Statistical significance was determined by a one-way ANOVA and Tukey's multiple comparison test (NS: not significant). Bar graphs show mean ± SD.

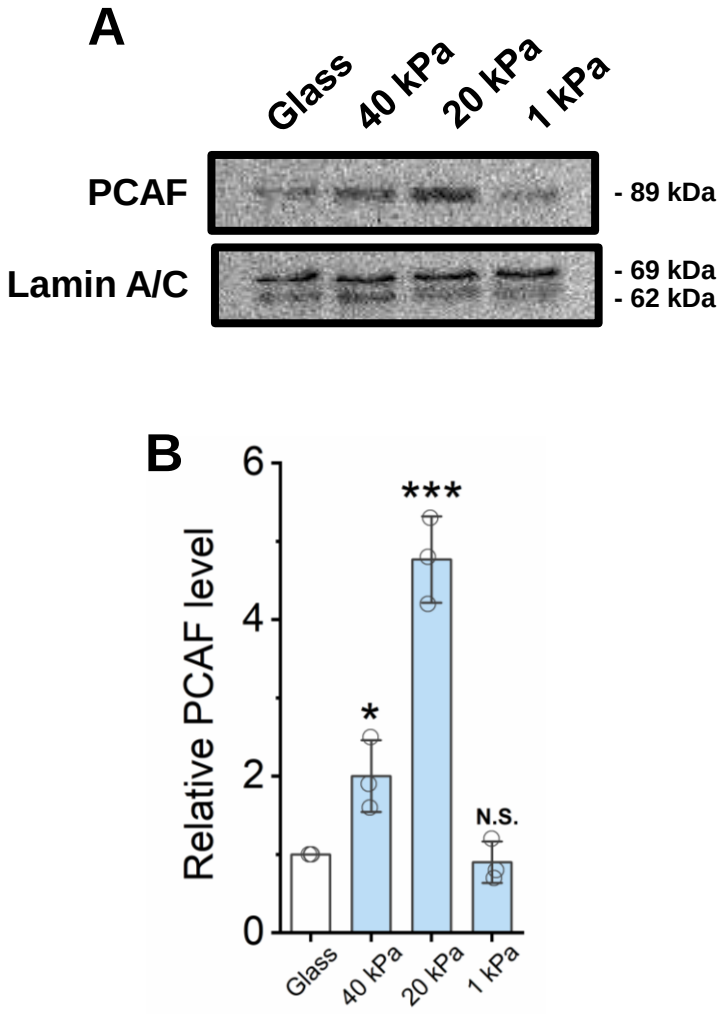

Fig. S27. Effect of matrix stiffness on PCAF translocation into nucleus. (A) Western blotting analysis shows PCAF levels from nuclear fractions of fibroblasts cultured on glass and PAAm gels of varying stiffness for 2 days where lamin A/C serves as a housekeeping protein (n=3). Nuclear proteins were isolated using the EpiQuik™ Nuclear Extraction Kit. **(B)** Quantification of PCAF level from Western blots in **A** (n=3), where protein levels were normalized to lamin A/C. Cells seeded on glass served as a control. Statistical significance was determined by a one-way ANOVA and Tukey's multiple comparison test (NS: not significant, *$p<0.05$, ***$p<0.001$). Bar graphs show mean ± SD.

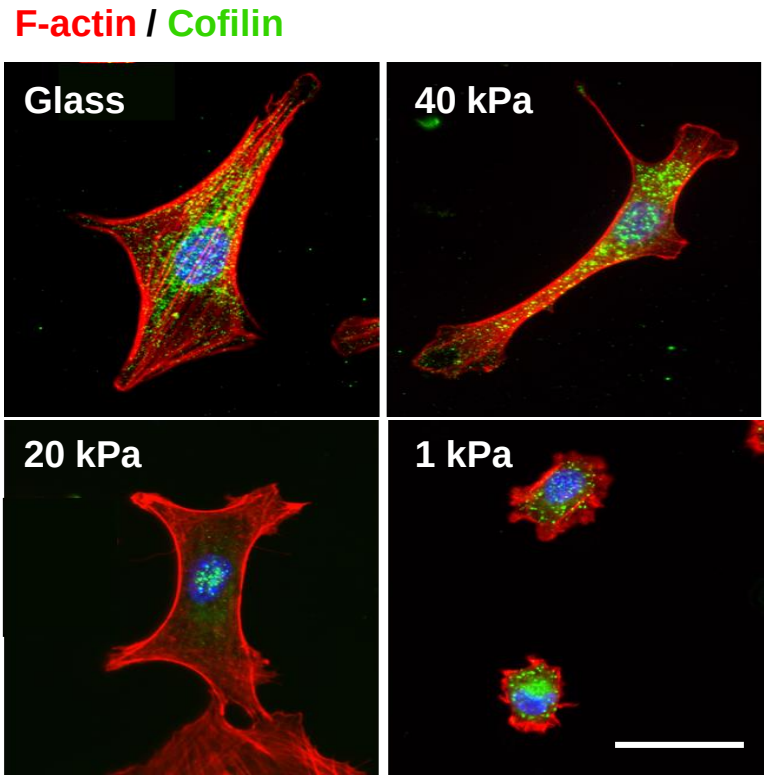

Fig. S28. Matrix stiffness modulates the assembly and nuclear translocation of cofilin. Immunofluorescent images of F-actin (phalloidin, red) and cofilin (green) in fibroblasts cultured on glass and PAAm gels of various stiffness for 2 days. Scale bar, 50 μm.

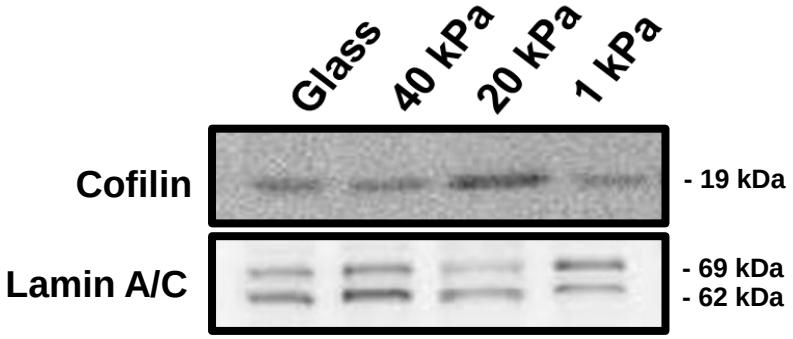

Fig. S29. Matrix stiffness modulates cofilin translocation. Western blotting analysis shows cofilin levels from nuclear fractions of fibroblasts cultured on glass and PAAm gels of varying stiffness for 2 days where lamin A/C serves as a housekeeping protein (n=3). Nuclear proteins were isolated using the EpiQuik™ Nuclear Extraction Kit.

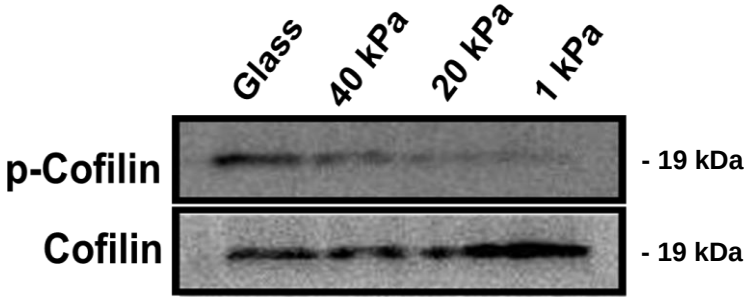

Fig. S30. Effect of matrix stiffness on phospho-Cofilin level. Western blotting analysis of phospho-Cofilin (Ser3) level from whole-cell lysates of fibroblasts cultured on fibronectin-coated glass and PAAm gels with varying stiffness for 48 hours, where cofilin level serves as the control.

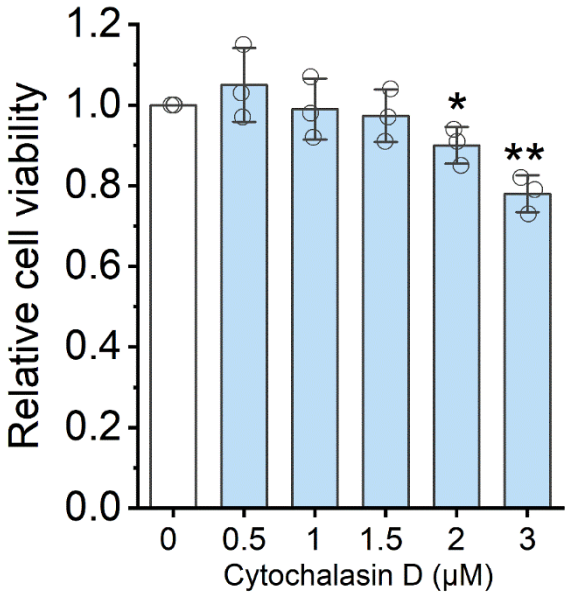

Fig. S31. Effect of actin polymerization inhibition on cell viability. Quantification of cell viability in fibroblasts treated with vehicle control (DMSO) or different doses of actin polymerization inhibitor, Cytochalasin D, for 24 hours, as determined by the PrestoBlue assay (n=3). Statistical significance was determined by a one-way ANOVA and Tukey's multiple comparison test (*p<0.05, **p<0.01). Bar graph shows mean ± SD.

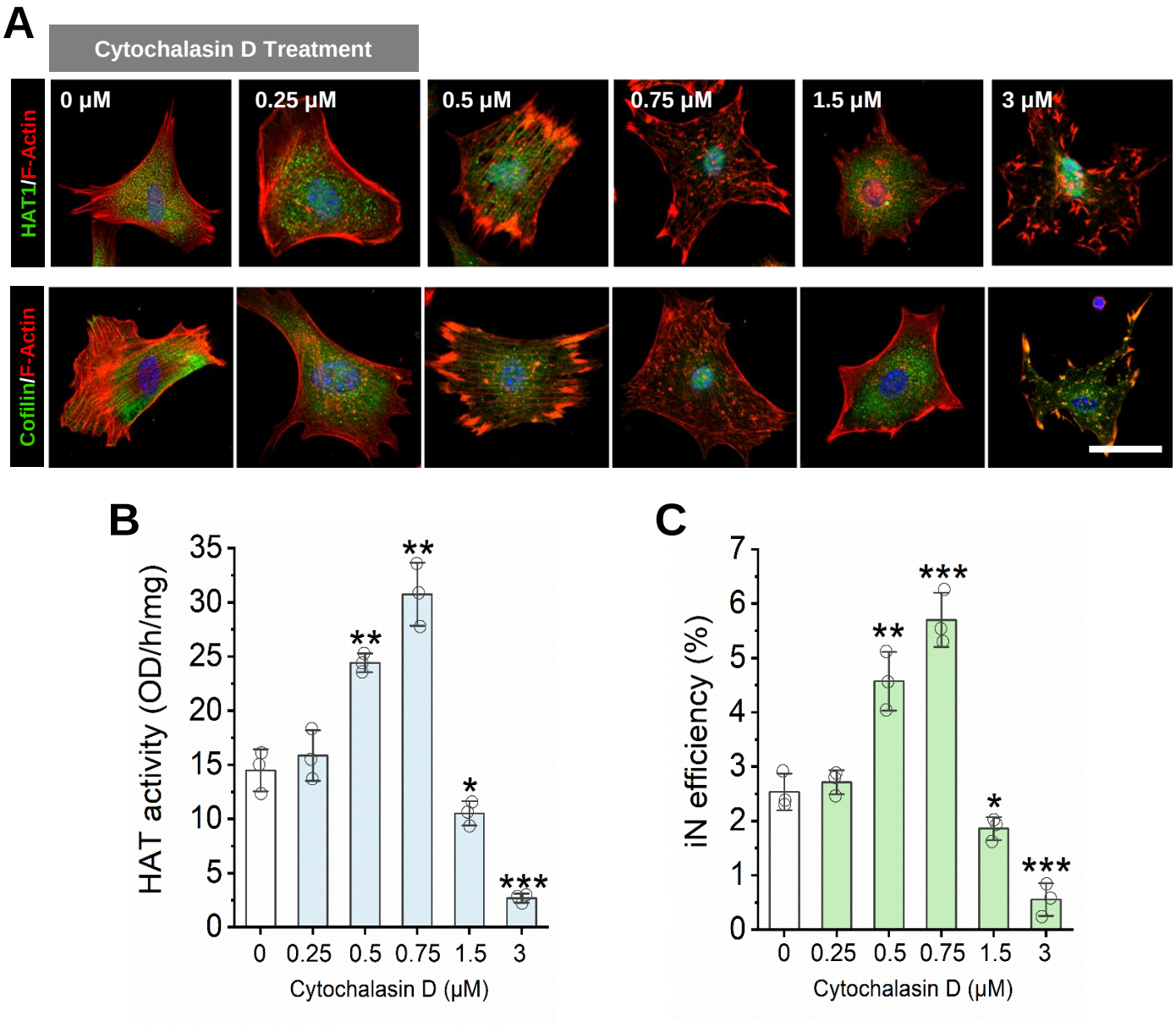

Fig. S32. Disruption of actin polymerization modulates cofilin translocation, HAT activity and iN reprogramming. (A) Representative immunofluorescent images of F-actin (phalloidin, red) with HAT1 (green; top panel) or cofilin (green; bottom panel) in BAM-transduced fibroblasts treated with different doses of actin polymerization inhibitor, Cytochalasin D for 24 hours. Scale bar, 50 μm. **(B)** Quantification of HAT activity in fibroblasts treated with vehicle control (DMSO) or different doses of cytochalasin D for 24 hours (n=3). **(C)** Reprogramming efficiency of BAM-transduced fibroblasts treated with varying doses of Cytochalasin D for 24 hours before the addition of Dox (n=3). Statistical significance was determined by a one-way ANOVA and Tukey's multiple comparison test (*p<0.05, **p<0.01, ***p<0.001). In **B** and **C**, bar graphs show mean ± SD.

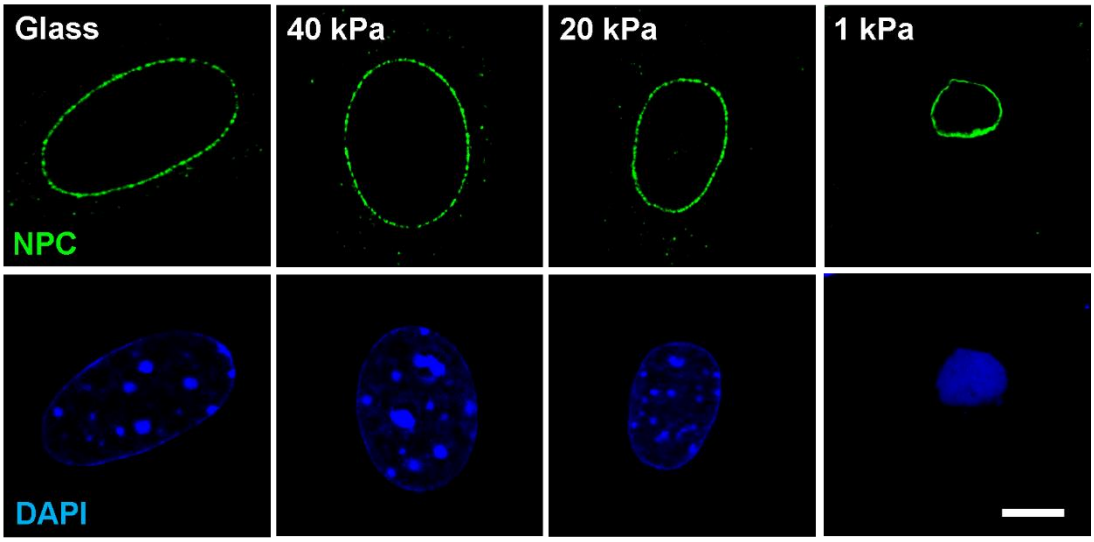

Fig. S33. Effect of matrix stiffness on nuclear pore complexes (NPCs). Immunofluorescent images of NPCs (green) and nuclei (DAPI, blue) in fibroblasts cultured on glass and PAAm gels of various stiffness for 2 days. Scale bar, 10 μm.

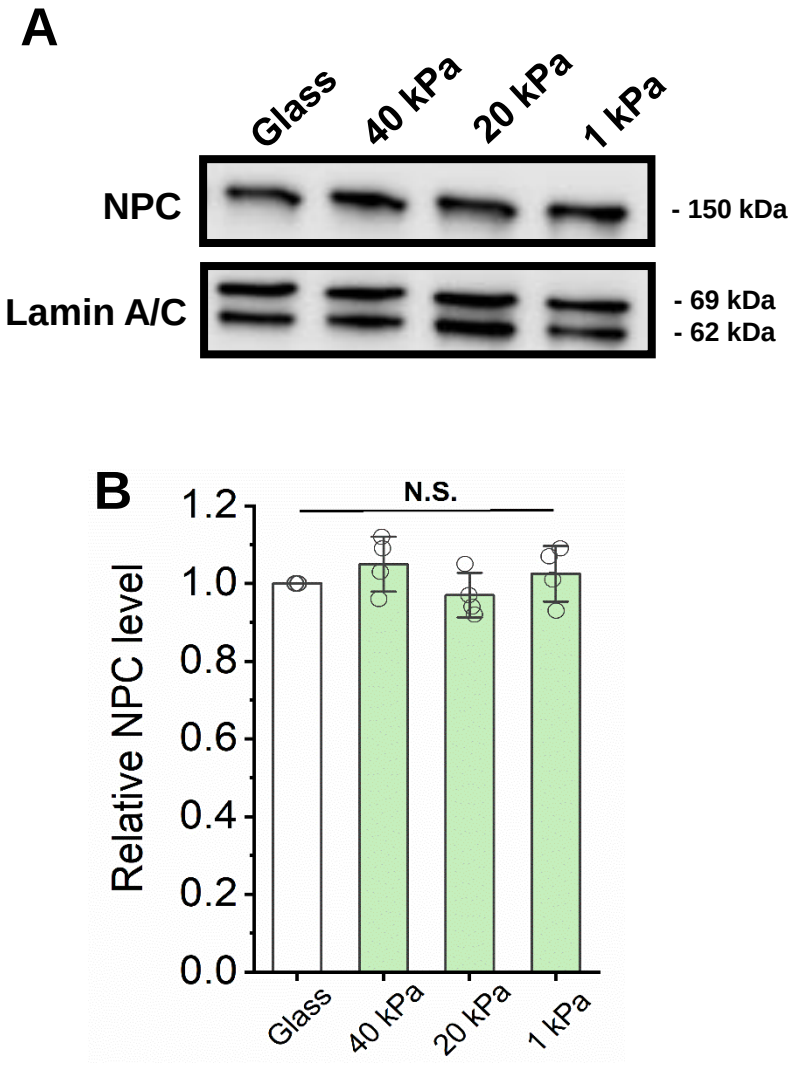

Fig. S34. Effect of matrix stiffness on nuclear pore complex (NPC) levels. (a) Western blotting analysis shows NPC levels from whole cell lysates of fibroblasts cultured on glass and PAAm gels for 2 days, where lamin A/C acts as housekeeping protein. **(b)** Quantification of NPC level from Western blots in **a** (n=4), where protein levels were normalized to lamin A/C. Cells seeded on glass served as a control. Statistical significance was determined by a one-way ANOVA and Tukey's multiple comparison test (NS: not significant). Bar graph shows mean ± SD.

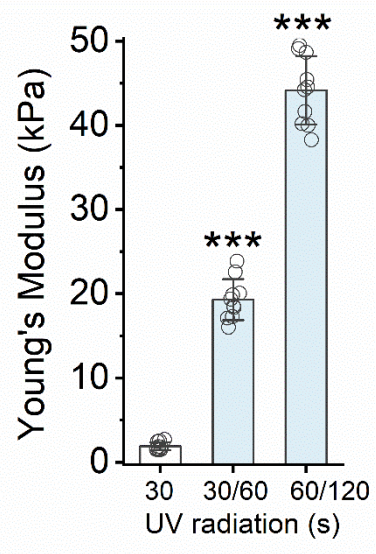

Fig. S35. Elastic modulus of dynamically tunable methacrylated hyaluronic acid (Me-HA) gels. Young's modulus of dynamically tunable uncoated Me-HA gels after sequential exposure to UV radiation, as determined by atomic force microscopy (AFM). Tunable gels were initially UV radiated for 30 seconds and 60 seconds, and then further radiated for 60 or 120 seconds, respectively. An AFM colloidal probe (sphere Ø = 3.5 μm) was utilized for the measurements and the Hertz model was used for data analysis. Tunable gels radiated with UV for only 30 seconds (no further UV exposure) served as a control. Statistical significance was determined by a one-way ANOVA and Tukey's multiple comparison test (n=10; ***$p<0.001$). Bar graph shows mean ± SD.

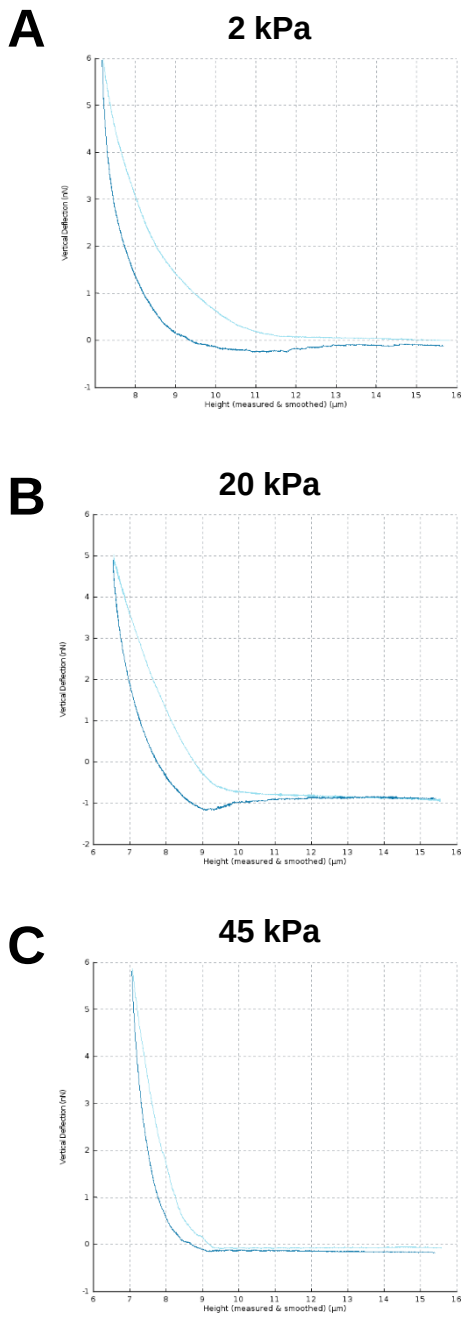

Fig. S36. Force-Distance (F-D) curves for tunable MeHA gels. (A-C) Representative F-D curves for dynamically tunable uncoated Me-HA gels after sequential exposure to UV radiation, as determined by AFM. Tunable gels were radiated with UV for only 30 seconds (no further UV exposure) to obtain 2 kPa gels. Tunable gels initially UV radiated for 30 seconds and 60 seconds, and then further radiated for 60 or 120 seconds, respectively, yielded 20 kPa and 45 kPa gels, respectively. An AFM colloidal probe (sphere Ø = 3.5 µm) was utilized for the measurements and the Hertz model was used for data analysis.

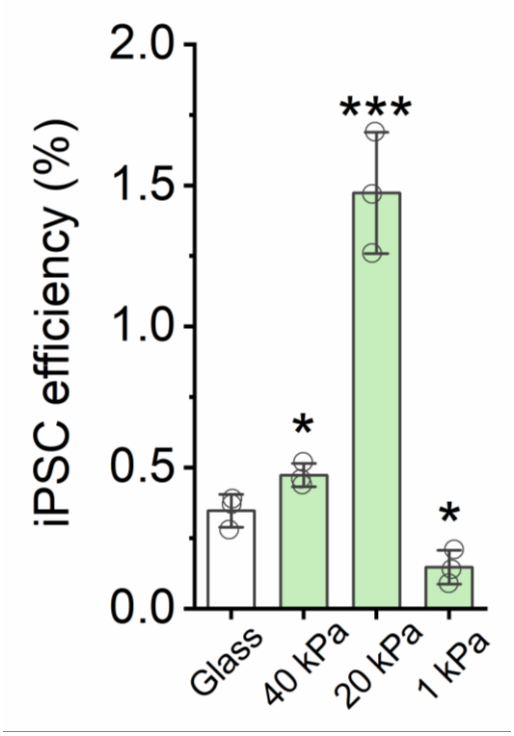

Fig. S37. Effect of substrate stiffness on iPSC reprogramming. Reprogramming efficiency of OSKM (Oct-4, Sox2, KLF4 and c-Myc)-transduced fibroblasts cultured on PAAm gels of varying stiffness (n=3). At day 21, the cells were fixed and stained for Nanog, followed by immunofluorescence microscopy to quantify $Nanog^+$ colonies. The reprogramming efficiency was determined by calculating the percentage of $Nanog^+$ colonies out of the cell numbers seeded at the beginning. Cells cultured on glass were kept as a control. Statistical significance was determined by a one-way ANOVA and Tukey's multiple comparison test (*$p<0.05$, ***$p<0.001$). Bar graph shows mean ± SD.

Fig. 3B

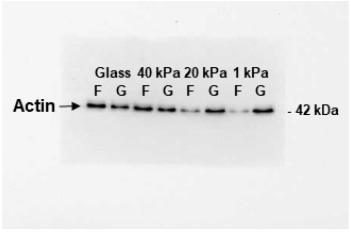

Fig. 3D (top)

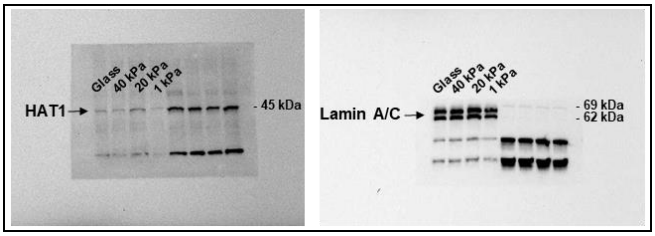

Fig. 3D (bottom)

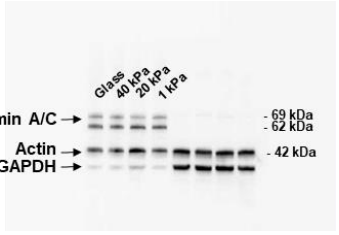

Fig. 3G

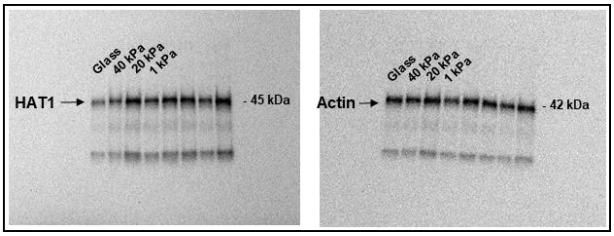

Fig. 4C

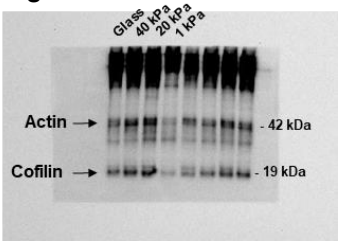

Fig. 4H

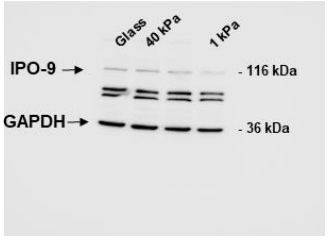

Fig. S26

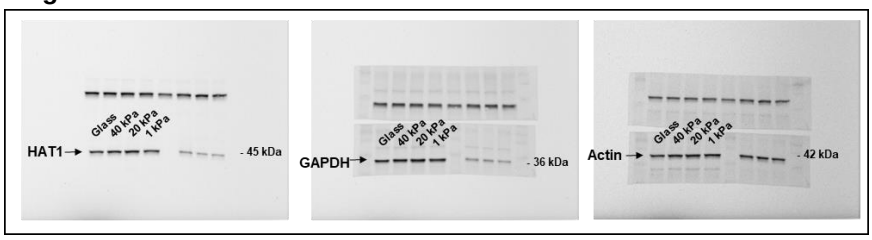

Fig. S27

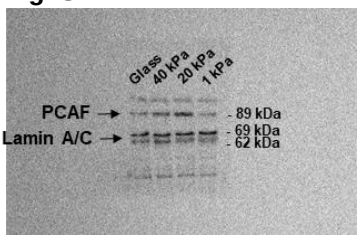

Fig. S29

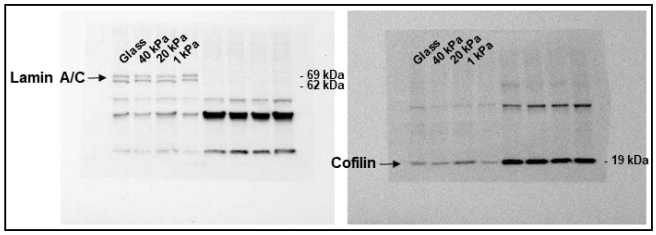

Fig. S30

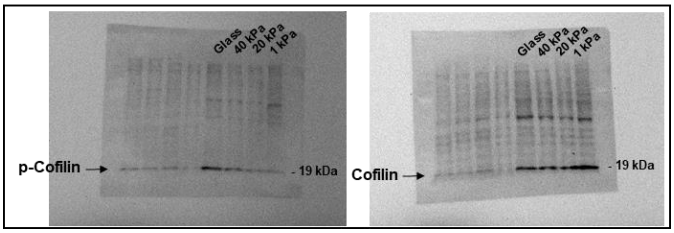

Fig. S34

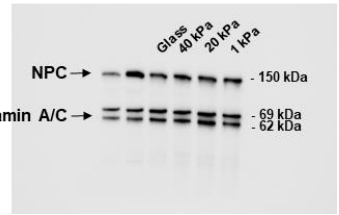

Fig. S38. Original blots for Western blot figures.

Table S1. Antibodies used for immunocytochemistry and Western blotting analysis

Antibody	Vendor	Catalog #	Dilution
Tuj1 (Tubb3)	Biolegend	801202	1:1000 (IF)
H3K4me3	Cell signaling	5326S	1:300 (IF)
H3K9me3	Abcam	ab8898	1:300 (IF)
H4K20me3	Abcam	ab4729	1:300 (IF)
H3K27me3	Abcam	ab192985	1:300 (IF)
H3K27ac	Abcam	ab4729	1:300 (IF)
AcH3	Millipore	06-599	1:300 (IF)
p-cofilin	Santa Cruz	sc-271921	1:500 (WB)
NeuN	Biolegend	834501	1:200 (IF)
Synapsin	Abcam	ab64581	1:100 (IF)
MAP-2	Sigma	M9942	1:200 (IF)
Lamin A/C	Santa Cruz	sc-376248	1:1000 (WB)
Histone H3	Santa Cruz	sc-8654	1:1000 (IF)
HAT1	Abcam	ab-184296	1:200 (IF)/ 1:1000 (WB)
Actin	Santa Cruz	sc-1616	1:200 (IF)/ 1:1000 (WB)
Cofilin	Cell signaling	5175S	1:300 (IF)/ 1:1000 (WB)
IPO-9	Invitrogen	PA1-41395	1:1000 (WB)
NPC	Biolegend	902902	1:200 (IF)/ 1:1000 (WB)
GAPDH	Santa Cruz	sc-32233	1:1000 (WB)
Paxillin	Abcam	ab32084	1:150 (IF)
PCAF	Santa Cruz	sc-13124	1:1000 (WB)
AcH4	Millipore	06-866	1:100 (IF)